Front. Earth Sci. 2021, 15(3): 631–648
https://doi.org/10.1007/s11707-020-0839-8

RESEARCH ARTICLE

Integration of 1D and 3D modeling schemes to establish the Farewell Formation as a self-sourced reservoir in Kupe Field, Taranaki Basin, New Zealand

S.M. Talha QADRI (✉)[1], Md Aminul ISLAM[2], Mohamad Ragab SHALABY[2,3], Syed Haroon ALI[4]

1 Department of Earth Sciences, University of Toronto, Toronto M5S2E8, Canada
2 Geosciences Program, Faculty of Science, Universiti Brunei Darussalam, Bandar Seri Begawan BE 1410, Negara Brunei Darussalam
3 Geology Department, Faculty of Science, Tanta University, Tanta 31527, Egypt
4 Department of Earth Sciences, University of Sargodha, Sargodha 40100, Pakistan

Abstract Along with conventional methods, this paper proposed a method in which 1D and 3D models are integrated to identify the self-sourced reservoir potential of the Farewell Formation in the Kupe Gas Field within the Taranaki Basin, New Zealand. Source rock characteristics were evaluated at both field and basin scales by investigating source rock maturity, type of organic matter, and hydrocarbon generation potential by rock pyrolysis, using Rock-Eval 2 and 6. The 1D thermal and burial history model established the rate of sedimentation and thermal history of the Kupe 4 well. Reservoir characterization at field-scale was determined by seismic interpretation, well log analysis, and 3D structural and petrophysical models. The sediments of the Farewell Formation contain types II-III (oil/gas prone) and type III (gas prone) and have fair-to-excellent generation potential. The oxygen and hydrogen indices ranged from 3 to 476 mg CO_2/g *TOC* and 26 to 356 mg HC/g *TOC*, respectively, whereas the thermal maturity determined by vitrinite reflectance values ranged between 0.3% and 0.72%, indicating that the Farewell Formation is in immature-to-mature hydrocarbon generation stage. Thus, Farewell Formation was verified to be a good source rock. Additionally, structural interpretations demonstrated the structural complexity of an extensional and contractional regime within the reservoir package. Multiple faults indicated a good reservoir property there with a trapping mechanism as well as migration paths. A well-log-based petrophysical analysis established the presence of up to 70% hydrocarbon saturation within the pore spaces of Farewell sandstones. The 3D models confirmed that the Farewell Formation has significant sand zones and hydrocarbon-saturated zones, thereby proving its very good reservoir characteristics. It has been proved that the 1D and 3D structural schemes, integrated with geological techniques, was vital in identifying the Kupe Field as a self-sourced reservoir.

Keywords self-sourced reservoir, Kupe Field, Farewell Formation, Taranaki Basin

1 Introduction

Improvements in technology and living standard have triggered a massive increase in fossil fuel consumption and concomitant discoveries of hydrocarbon fields (Adelu et al., 2019). To meet the global energy requirements, the focus of hydrocarbon exploration industry has shifted from conventional tools and targets to advanced tools and complex geological settings (Osinowo et al., 2018, Islam et al., 2020). This paradigm shift, initiated the integration of geological, geophysical, geostatistical, and petrophysical data sets for source and reservoir characterization, is essential to resource development (Seyyedattar et al., 2020). The Cretaceous-Cenozoic Taranaki Basin is abundant with plentiful oil and gas resources and has a long history of hydrocarbon production (King and Thrasher, 1996). The Kupe Field is a gas condensate field located offshore in the southern Taranaki Basin (Fig. 1; Knox, 1982). The Farewell Formation comprises primarily fluvial sandstones; however, within the Kupe Field, a substantial quantity of carbonaceous and coaly material is observed in the deeper sections (Killops et al., 1994).

Numerous studies have been conducted to investigate various aspects of the source and reservoir formations,

Received April 13, 2020; accepted October 8, 2020

E-mail: talhaqadri_uos@hotmail.com

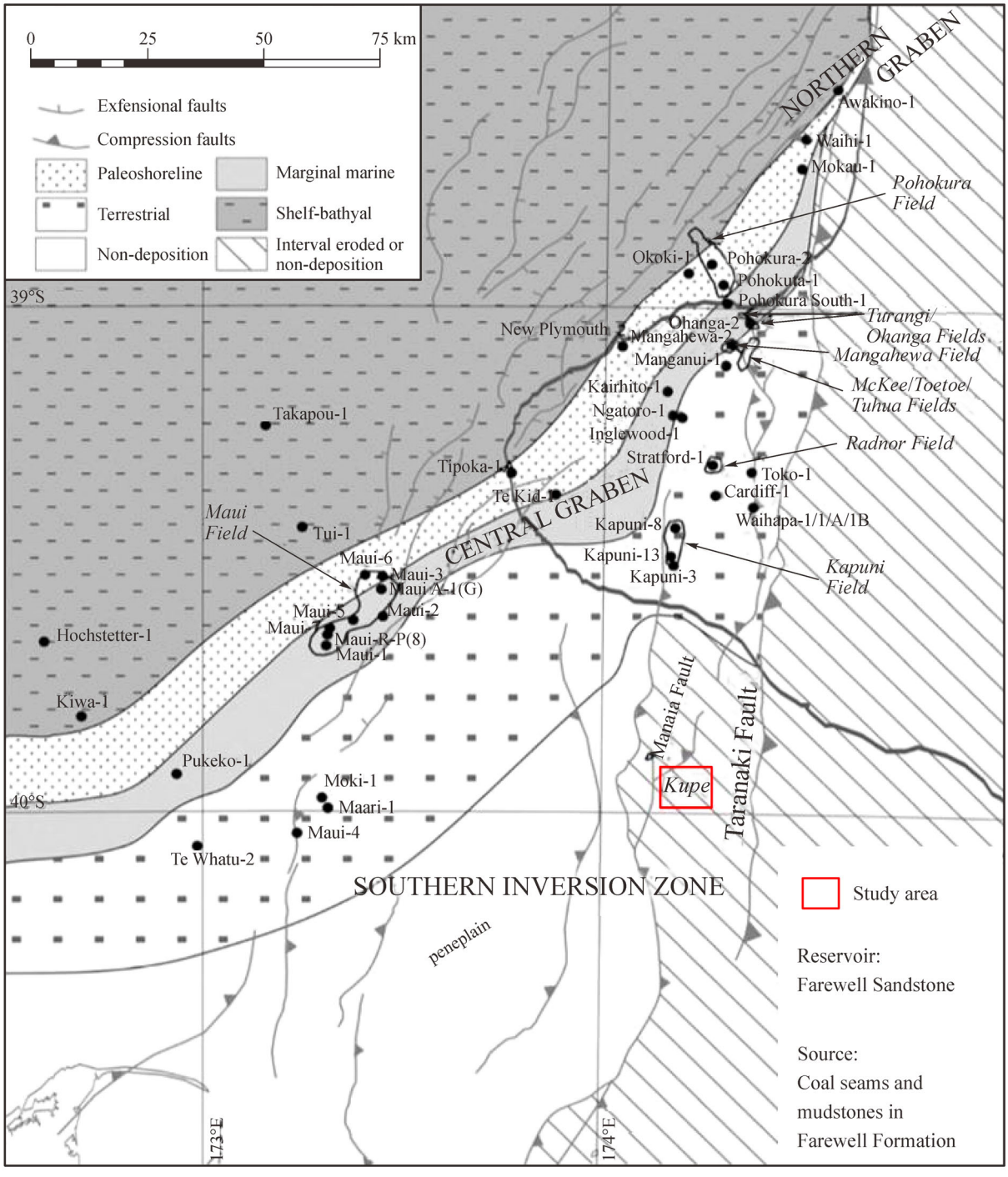

Fig. 1 The map shows Kupe Field (red square) bounded by Taranaki Fault and Manaia Fault within the southern inversion zone of the Taranaki Basin. The Northern Graben and Central Graben along with multiple other oil and gas fields are also shown (modified after Higgs et al., 2012).

mostly on a basin-scale, within the Taranaki Basin (e.g., Thompson, 1982; Killops et al., 1994; Martin et al., 1994; Armstrong et al., 1996; King and Thrasher, 1996; Sykes and Snowdon, 2002; Hemming-Sykes, 2011; Higgs et al., 2012; Ilg et al., 2012; Sykes et al., 2014; Sarma et al., 2014; Qadri et al., 2016; Haque et al., 2016; Qadri et al., 2017; Higgs et al., 2017; Jumat et al., 2018; Qadri et al., 2019a; Franzel and Back, 2019, Islam et al., 2020, Qadri et al., 2020). However, hardly any of the studies have highlighted the self-sourced reservoir potential of the

Farewell Formation on a field or regional scale within the Taranaki Basin. This provided an impetus for the present integrated study of the identification and evaluation of the Farewell Formation as a self-sourced reservoir within the Kupe Field. The study is based on two aspects, i.e., the evaluation and characterization of the source rock, and characterization of the reservoir of the Farewell Formation in the Kupe Gas Field. The maturity, type of organic matter, hydrocarbon generation potential, and thermal burial history were investigated using geochemical data obtained from various fields, including the Kupe Gas Field, to characterize the source rock of the Farewell Formation. Moreover, the second part of the investigation used 3D seismic volume, well log data for the structural interpretation, well log analysis, and 3D reservoir modeling to establish the reservoir characteristics of the Farewell Formation.

2 Geological setting

The Taranaki Basin is located on the northern island of New Zealand, covers an area of approximately 100000 km^2 and contains the largest hydrocarbon accumulations in the country (King and Thrasher, 1996). The Taranaki Basin commenced as a rift basin during the Middle Cretaceous to the Paleocene and transformed into a passive continental margin during the Eocene to Early Oligocene period. During the Miocene era, the Taranaki Basin developed as a foreland, and from the Late Miocene to recent time, it transformed into a back-arc basin (Franzel and Back, 2019). The Taranaki Basin is divided into two structural provinces: The Eastern Mobile platform, which has undergone tectonic activity, and the Western Stable Platform, which has experienced negligible disturbances since the Eocene (Knox, 1982). The Eastern mobile platform is further subdivided into northern, central, and southern graben. The northern and central grabens have experienced extensional tectonics, whereas the southern graben (also called the southern inversion zone) indicates structural inversion (King and Thrasher, 1996). The study conducted by Knox (1982) demonstrated that the extensional stage in the northern graben was concurred with the compressional stage in the south graben. Furthermore, the southern inversion is subdivided into three zones: Zones A, B, and C. The Kupe Field is in zone A of the southern inversion structures, resulting from the tectonic process initiated during the Late Miocene (Qadri et al., 2017, Franzel and Back, 2019). The fault-bounded Kupe Field has accumulated hydrocarbons within the Paleocene fluvial sandstones (Martin et al., 1994). The detailed stratigraphic succession (Fig. 2) of the Taranaki Basin is divided into 6 groups: Pakawau, Kapuni, Moa, Ngatoro, Wai-iti, and Rotokare groups (King and Thrasher, 1996). The present study focuses on the Farewell Formation — a member of the Kapuni group, deposited during the tectonic quiescence of the Palaeogene, and dominated by sandstones and lower floodplain coal measures with some shales (Johnston et al., 1990).

3 Data and methods

The data sets used in the study were provided and permitted for publication by the Ministry of Business, Innovation and Employment (MBIE) of New Zealand and GNS Sciences (New Zealand) (Sykes et al., 2014). The data sets included 45 drill cutting samples of the Farewell Formation from 9 wells: Cook-1, Fresne-1, Kupe-1, Kupe South-2, Kupe South-5, Maui-3, Maui-4, North Tasman-1, and Pukeko-1 (Table 1). Coal, claystone, mudstone, and shale were the important lithological constituents of these samples. Table 1 shows that 33.3% of these samples were coal, 26.6% were claystone (all in Kupe-1 well), 22.2% were mudstone, and 17.7% were shale. In addition, 3D seismic volume, well-log data, check-shot deviation surveys, and well-completion reports were also used to comprehend the reservoir features of the Farewell Formation. The structural model used 6 wells, namely Kupe 1, Kupe South 3B, Kupe 4, Kupe 6, Kupe 7-ST, and Kupe South 8, whereas the well log analysis and the petrophysical model incorporated four wells, namely Kupe 1, Kupe South 3B, Kupe South 7ST, and Kupe South 8.

Pyrolytic analyses were conducted using Rock-Eval 2 and 6 to investigate the maturity of source rock, type of organic matter, and hydrocarbon generation potential. The rock pyrolysis scheme allowed the evaluation of important parameters to characterize the source rock, i.e., the volume of free hydrocarbon present in the source rock before pyrolysis (S_1), amount of hydrocarbon found during pyrolysis (S_2), amount of CO_2 liberated (S_3), and total organic carbon content (*TOC*). The maturity of the source rock was estimated by plotting vitrinite reflectance (R_o, %) against the maximum temperature during pyrolysis (T_{max}) for 15 samples (Espitalie et al., 1977). Other important source rock parameters were also derived from the abovementioned parameters, including the hydrogen index ($HI = (S_2/TOC) \times 100$), oxygen index ($OI = S_3/TOC) \times 100$), and production yield ($PY = S_1 + S_2$) (Tissot and Welte, 1984; Peters, 1986; Mukhopadhyay, 1994). These important source rock parameters are presented in Table 1. 1D burial modeling is an important approach for comprehending the burial history of sedimentary strata (Wapples, 1980 and 1994; Burrus et al., 1991). Various scientists have developed burial histories for multiple source rock formations in the Taranaki Basin (e.g., Armstrong et al., 1996; Sarma et al., 2014, Qadri et al., 2016; Jumat et al., 2018). Schlumberger PetroMod (version 9.1) was used to develop a 1D thermal-burial history simulation for the Farewell Formation in the Kupe 4-well. The software uses information such as formation names, formation thickness (m), age (Ma), depth (m), and

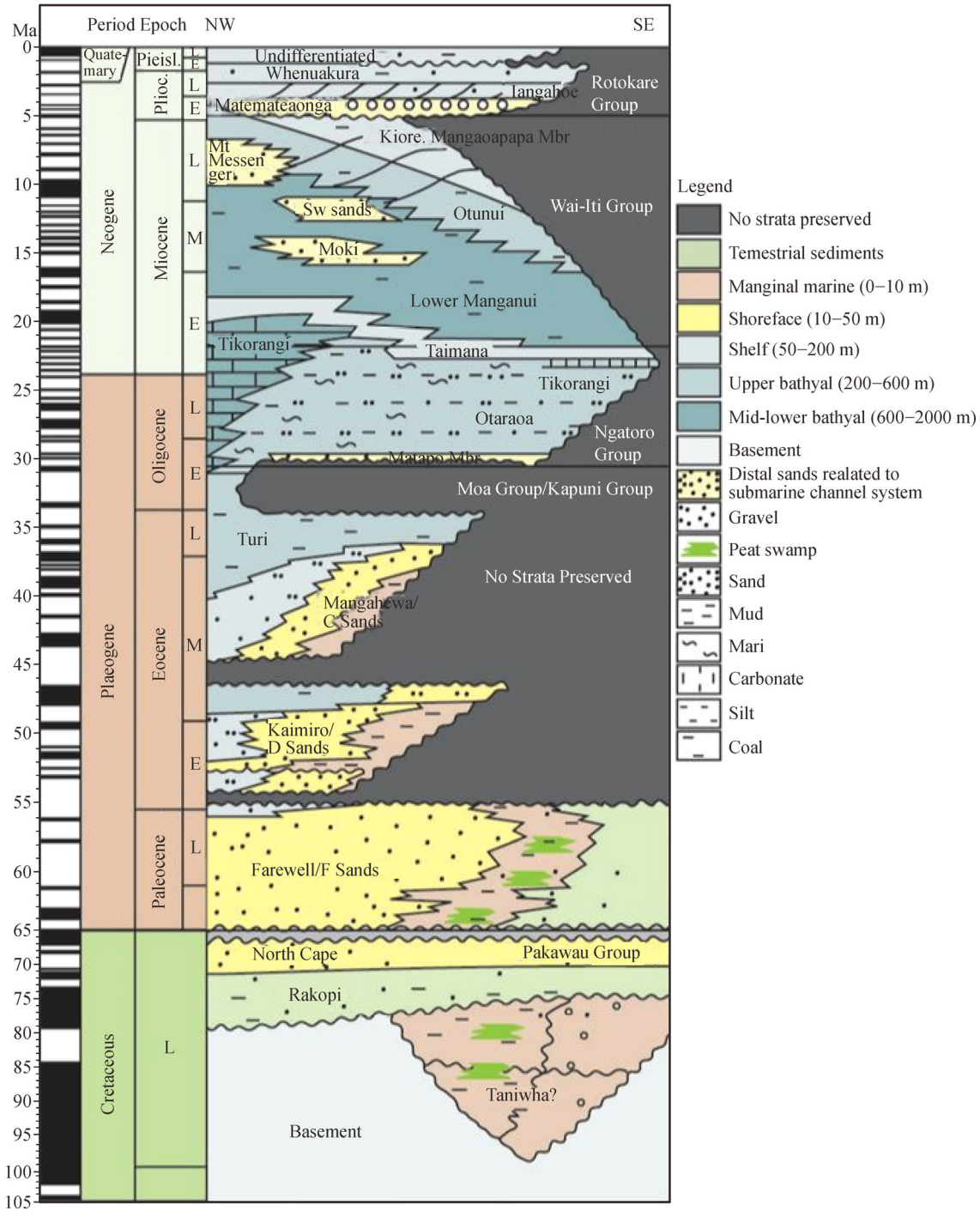

Fig. 2 The generalized stratigraphic succession showing multiple groups and formation within the Taranaki Basin (modified after Martin et al., 1994).

lithology (Table 2) obtained from well completion reports and composite well data.

The Interactive Petrophysics 2013 software (LR Synergy) was used to conduct quantitative well log analyses. The data from Kupe South 1, Kupe South-3B, Kupe South-7ST, and Kupe 8 wells were used to determine petrophysical parameters, including total porosity, effective porosity, shale water volume, and hydrocarbon saturation. Porosity was evaluated using Wyllie's equation (Wyllie, 1963), which uses neutron, density, and sonic log values. The shale content and its type of distribution were identified using gamma-ray, neutron, neutron-density

Table 1 Rock-Eval analysis used in the present study

Well	Depth	Sample	Lithology	S_1	S_2	S_3	T_{max}	*OI*	*HI*	*TOC*	*PI*	S_2/S_3	R_o
	1487	Cuttings	Mudstone	0.15	0.72	0.87	434	95	79	0.91	0.17	0.82	0.65
	2343	Core	Shale	0.1	1.9	0.2	432	16	152	1.25	0.05	9.5	
	2508	Cuttings	Shale	2.67	52.8	4.14	431	25	323	16.3	0.05	12.75	
Cook-1	2587	Cuttings	Shale	1.3	24.53	1.47	429	21	359	6.83	0.05	16.68	
Cook-1	2667	Cuttings	Shale	0.98	17.48	2.35	431	29	220	7.94	0.05	7.43	
Cook-1	2271	Cuttings	Mudstone	2.4	38.5	3.9	427	31	306	12.6	0.06	9.87	0.52
Cook-1	2342	Cuttings	Mudstone	0.2	1.3	0.17	425	33	241	0.54	0.13	7.64	0.47
Cook-1	2576	Cuttings	Mudstone	4.5	53.1	4.82	430	24	264	20.1	0.08	11.01	
Cook-1	2579	Cuttings	Mudstone	3.9	72	5.35	431	20	271	26.6	0.05	13.45	0.6
Cook-1	2643	Cuttings	Coal	4.5	72.7	7.12	437	19	198	36.7	0.06	10.21	0.72
Cook-1	2673	Cuttings	Coal	2.4	29.2	4.14	432	11	92	39.1	0.08	7.05	0.63
Fresne-1	785	Cuttings	Shale	0.17	2.53	0.83	433	75	230	1.1	0.06	3.04	
Kupe S-2	3180	Cuttings	Coal	7.9	181.1	24.9	435	32	233	77.6	0.04	7.27	
Kupe S-2	3195	Core	Mudstone	0.51	12.97	1.53	432	29	252	5.15	0.04	8.47	
Kupe S-2	3200	Core	Mudstone	0.03	2.99	0.34	439	33	294	1.02	0.01	8.79	
Kupe S-5	2914	Core	Coal	1.27	84.55	28.8	423	50	147	57.91	0.01	2.93	0.5
Kupe S-5	2915	Core	Mudstone	0.16	10.2	2.63	438	52	204	5	0.02	3.87	
Kupe S-5	2939	Cuttings	Coal	1.5	55.8	46.9	430	66	79	70.3	0.03	1.18	0.58
Kupe S-5	3182	Cuttings	Coal	1.7	76.2	41.5	426	57	105	72	0.02	1.83	0.54
	3233	Cuttings	Claystone	0.25	0.63	3.24	428	476	92	0.68	0.28	0.19	
	3261	Cuttings	Claystone	0.22	0.70	0.71	426	304	104	0.68	0.24	0.98	
	3291	Cuttings	Claystone	0.22	0.66	0.66	430	384	88	0.75	0.25	1	
	3322	Cuttings	Claystone	0.26	0.53	0.53	424	294	79	0.67	0.33	1	0.3
Kupe-1	3352	Cuttings	Claystone	0.08	0.43	0.44	433	204	52	0.84	0.15	0.97	
Kupe-1	3383	Cuttings	Claystone	0.24	0.5	0.5	415	313	52	0.95	0.32	1	
Kupe-1	3416	Cuttings	Claystone	0.21	1.75	1.76	435	141	80	2.2	0.11	0.99	
Kupe-1	3447	Cuttings	Claystone	0.17	2.64	2.64	436	93	88	2.98	0.06	1	
Kupe-1	3505	Cuttings	Claystone	0.26	1.38	1.38	433	108	92	1.49	0.16	1	
Kupe-1	3535	Cuttings	Claystone	0.22	2.54	2.49	435	82	96	2.6	0.08	1.02	
Kupe-1	3566	Cuttings	Claystone	0.18	1.498	1.49	434	153	80	1.86	0.11	1.01	
Kupe-1	3599	Cuttings	Claystone	0.21	2.73	2.71	434	121	100	2.69	0.07	1.01	
Kupe-1	3627	Cuttings	Coal	0.24	3.22	3.22	435	83	90	3.57	0.07	1.0	0.67
Kupe-1	3657	Cuttings	Coal	0.13	1.16	1.13	431	128	69	1.63	0.1	1.02	0.6
Maui-3	3319	Cuttings	Shale	0.26	0.47	0.65	429	70	51	0.92	0.36	0.72	
Maui-3	3398	Cuttings	Shale	0.21	0.22	0.95	426	114	26	0.83	0.49	0.23	
	2228	Cuttings	Coal	2.74	30.65	6.25	423	47	233	13.15	0.08	4.90	
	2410	Cuttings	Shale	1.38	7.78	2.53	423	56	174	4.46	0.15	3.07	
Maui-4	2505	Cuttings	Coal	2.79	111.4	20.53	428	30	163	69.09	0.02	5.43	
Maui-4	2505	Cuttings	Coal	2.29	71.51	8.91	427	31	252	28.56	0.03	8.02	
Maui-4	2505	Cuttings	Mudstone	0.61	21.22	2.52	427	31	266	8.02	0.03	8.42	
Maui-4	2670	Cuttings	Coal	2.73	116.3	19.73	428	28	168	69.89	0.02	5.89	
Maui-4	2670	Cuttings	Coal	1.45	52.07	9.23	428	30	170	30.9	0.03	5.64	
N Tasman-1	2202	Cuttings	Mudstone	1.3	42.9	7.6	429	58	330	13	0.03	5.64	0.55
Pukeko-1	3940	Cuttings	Coal	10.6	224.6	1.99	418	3	344	65.62	0.05	112.8	0.59
Pukeko-1	4005	Cuttings	Coal	8.33	176.3	2.09	417	4	336	52.76	0.04	84.39	0.59

Table 2 Input parameters for the 1D thermal burial history model for Kupe-4 well.

Formation name	Age/Ma	Top/m	Bottom /m	Thickness/m	Lithology	Petroleum system elements
Surficial deposits	0.5–Recent	0	68.1	68.1	Recent sediments	Overburden rock
Giant foresets	2.5–0.5	68.1	1000	932	Sandstone with interbedded mudstone	Overburden rock
Tangahoe	4.0–2.5	1000	1257	257	Mudstone	Overburden rock
Matemateaonga	6.0–4.0	1257	1768	568	Mixed package of sandstone, siltstone, and mudstone	Overburden rock
Manganui	20.5–6.0	1768	2564	796	Claystone	Overburden rock
Taimana	22–20.5	2564	2820	256	Calcareous siltstone	Overburden rock
Otaraoa	32–22	2820	3054	234	Claystone	Seal Rock
Farewell	63–56	3054	3334	280	Shaly sand and coal seams, and carbonaceous mudstones	Source Rock

porosity, and other combination logs (Hakimi et al., 2012). Owing to the presence of a dispersed type of shale habitat, a dual water saturation model was used for the precise calculation of fluids within the reservoir formation. Hydrocarbon saturation was estimated by subtracting the water saturation from 100% saturation (Hakimi et al., 2012; Ali et al., 2019; Qadri et al., 2019a, and 2019b).

The Schlumberger Petrel software was used for seismic interpretation to establish 3D structural and petrophysical models by incorporating 3D seismic volume, check-shots, and deviation-surveys from the Kupe Field. The top of the reservoir formation was identified by establishing well-to-seismic ties; a synthetic seismogram was designed by incorporating sonic and other well log data. Along with the reservoir horizon, multiple depositional packages and faults were also interpreted, which revealed different depositional sequences. Seismic facies were also considered by realizing multiple reflection patterns, indicating the reflection configuration and different depositional sequences (Weimer et al., 1988; Anyiam et al., 2020). Velocity modeling was performed to establish the structural framework model in the depth domain, followed by the initiation of the 3D grid surfaces of the reservoir tops in the Farewell Formation. These grid surfaces were used as the main input grids for developing the 3D petrophysical model. The petrophysical properties estimated from the well log analysis were filled into these grids to visualize the distribution of the petrophysical parameters throughout the reservoir surface. The interpolation of petrophysical properties was performed using a stochastic technique, termed as sequential Gaussian simulation. This stochastic technique provides a more normalized and realistic dissemination of petrophysical factors in the 3D petrophysical model. The distribution of shale and sand within the reservoir was shown by a 3D gamma-ray model, whereas the 3D gas saturation model demonstrated the significant distribution of hydrocarbons within the reservoir.

4 Results, analysis, and discussion

4.1 Source-rock evaluation and characterization

Results derived from the pyrolysis of the Farewell Formation demonstrated that S_1 ranged between 0.03 and 10.65 mg HC/g rock. S_2 and S_3 yields ranged from 0.22 to 224.64 mg HC/g rock and 0.17 to 46.9 mg HC/g rock, respectively. These samples also exhibited a high *TOC* content, ranging between 0.54% and 77.6%. The maximum pyrolysis temperature (T_{max}) was between 415°C and 439°C, whereas the vitrinite reflectance (R_o, %) ranged between 0.3% and 0.72%. The derived values of oxygen index (*OI*) fluctuated between 3 and 476 mg CO_2/g *TOC*, and hydrogen index (*HI*) fluctuated between 26 and 356 mg HC/g *TOC*. The production index (*PI*) ranged between 0.01 and 0.49. Several cross plots (Figs. 3–9) were generated to establish the type of organic matter, generation potential, and hydrocarbon maturity, as well as the origin, quality, and quantity of hydrocarbons within the source rock.

The origin of hydrocarbons found within the source rock was examined using the *TOC* versus S_1 plot. The examined samples from all the wells were uncontaminated, indicating that the hydrocarbons accommodated by the source rock are autochthonous and have not migrated from elsewhere (Fig. 3). The type of hydrocarbon expected to be produced was identified by plotting T_{max} against S_2/S_3 (Fig. 4). Most of the data sets are clustered around gas as well as (oil-gas) mixed zones (Fig. 4). Very few samples were observed in the oil zone. Most of the data from the Kupe Field were also observed in the gas window. The quality of organic matter observed in Fig. 4 occurs in the fair-to-excellent zone.

Kerogen type, quality, and thermal maturity were determined by plotting *OI* versus *HI* (Fig. 5) and T_{max} versus *HI* (Fig. 6). All samples were indicative of kerogen type II (oil-gas prone) and type III (gas prone) (Fig. 5). The

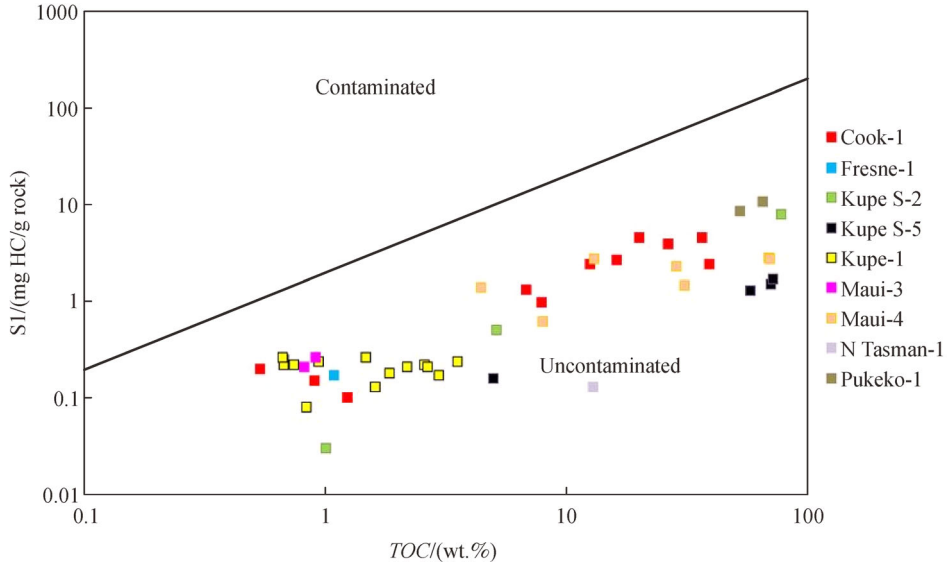

Fig. 3 The S_1 versus *TOC* crossplot indicating the origin of hydrocarbon in the Farewell Formation

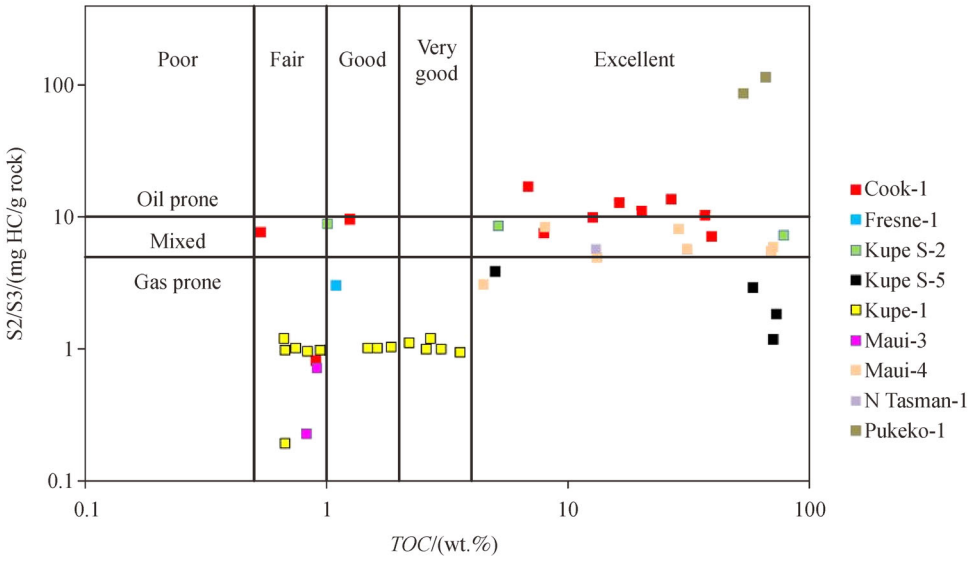

Fig. 4 The cross-plot showing *TOC* versus S_2/S_3 values indicating the quality and type of hydrocarbon expected to be generated from the analysed samples of the Farewell Formation.

studies conducted by Barker (1974), Peter and Cassa (1994), Sykes and Snowdon (2002), Shalaby et al. (2011), Qadri et al. (2016), and Osli et al. (2018) demonstrated that the mature oil window ranges from 430°C to 455°C. The maturity of organic matter was estimated by plotting T_{max} against *HI* (Fig. 6), and the samples obtained from the Farewell Formation lie mostly within the immature-to-mature zones. These samples were not observed within the condensate wet zones and dry-gas zones. This suggests that these samples from the Farewell Formation have not reached the mature phase. The findings from Figs. 4, 5, and 6 are in good agreement, indicating that most of the samples contain type II-III (oil-gas prone) and type III kerogens (gas prone). Figure 7 shows the relationship between the production index (*PI*) and T_{max} and demonstrates that the Farewell Formation samples were thermally immature-to-mature, and the data clusters reflect the mostly indigenous hydrocarbons. Data not lying within the indigenous window were because of the low pyrolysis T_{max} values. These data could have been displaced to the indigenous zone by employing additional time and thermal maturity. The thermal maturity of the sample was

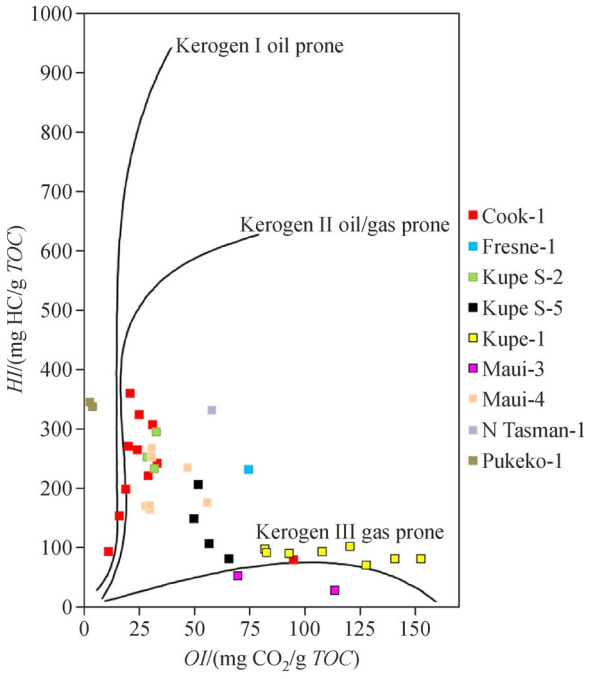

Fig. 5 A modified Van Krevelen diagram indicating the type of kerogen in the Farewell Formation encountered in multiple wells inlcuding wells from Kupe Field

determined by plotting pyrolytic T_{max} against the vitrinite reflectance data (Fig. 8). The values of vitrinite reflectance were highly dependent on the rapid temperature increment with burial depth and age of formation (Tissot and Welte, 1984; Peters, 1994; Peter and Cassa, 1986). Most of the samples lay within the thermally mature oil window, whereas a few samples were also observed in the immature phase (Fig. 8). Samples derived from Kupe-1 and Kupe S-5 wells exhibited a trend similar to samples derived from other wells located within the Taranaki Basin, analyzed in this study.

The thermal burial history for multiple stratigraphic successions, along with the rate of sedimentation, was modeled using the Schlumberger PetroMod 2013 software (Fig. 9). The parameters used to establish the 1D model are presented in Table 2. In the Kupe 4 well, the Farewell Formation resides over the North Cape Formation; the deposition started during the Paleocene era, approximately 63 Ma ago, and continued until the late Eocene, approximately 56 Ma, at a sedimentation rate of 40 m/year. The current thickness of the Farewell Formation is approximately 280 m. There is a hiatus between 56 and 32 Ma, indicating no preservation of any strata, specifically in the southeast of the Taranaki Basin. The Farewell Formation started subsiding with the deposition of the Otaraoa Formation between 32 and 22 Ma, with a sedimentation rate of 23.4 m/year, and its present thickness is 234 m in the Kupe 4 well. During the early Miocene (22.5–20 Ma), the Taimana Formation began depositing over the Otaraoa Formation, with a sedimentation rate of approximately 102 m/year, and presently has a thickness of 256 m. The Taimana Formation subsided underneath the Manganui Formation from 20 Ma, with an average sedimentation rate of 56.8 m/year, until the end of the late Miocene era (~ 6 Ma) and has a present-day thickness of 796 m. The Matemateaonga Formation was deposited over the Manganui Formation during 6–4 Ma, at a

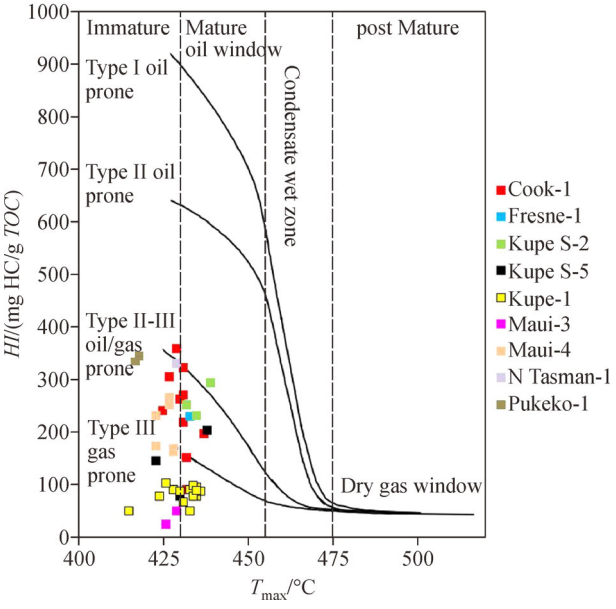

Fig. 6 A cross plot of T_{max} versus *HI* indicating source rock maturity and type of hydrocarbon from the analysed samples derived from Farewell Formation.

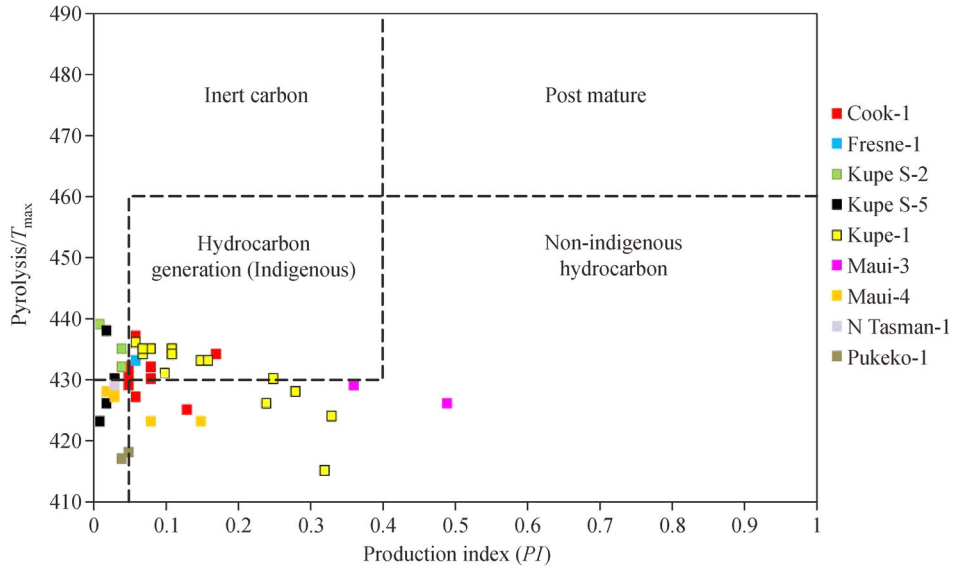

Fig. 7 The T_{max} versus PI cross plot indicating the maturity and nature of the hydrocarbon generation within the Farewell Formation samples.

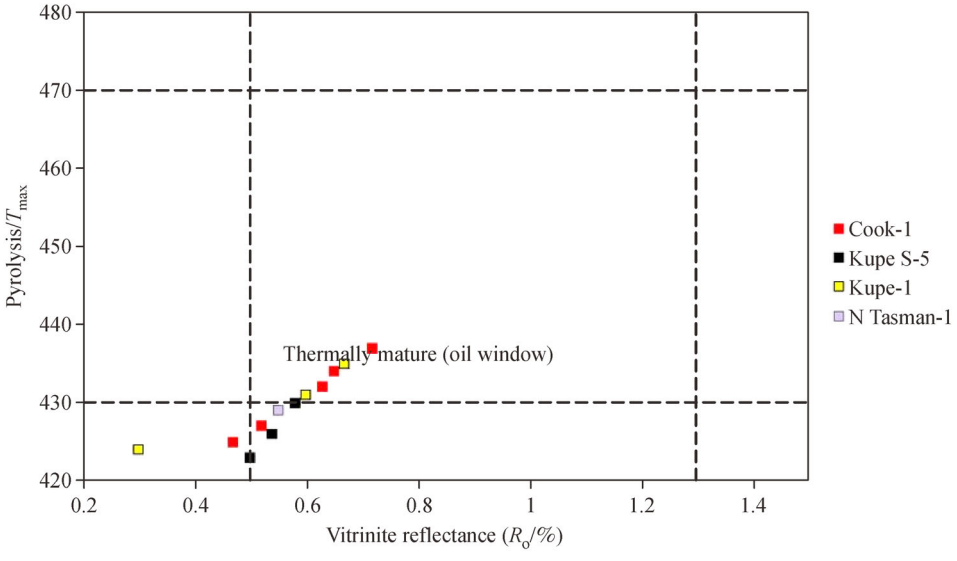

Fig. 8 The cross-plot between vitrinite reflectance and T_{max} data, indicating the thermal maturity of the analyzed samples from the Farewell Formation.

sedimentation rate of 284 m/year, and has a total thickness of 568 m in the Kupe 4 well. The Matemateaonga Formation started subsiding beneath the Tangahoe Formation in 4 Ma and continued till 2.5 Ma (early-to-late Pliocene era), with a sedimentation rate of approximately 171 m/year, and shows a thickness of 257 m in the Kupe 4 well. The Giant Foresets Formation was deposited during the late Pliocene era and the early Pleistocene era, with a high rate of sedimentation (466 m/year) and has a present-day thickness of 932 m within the well. Exposure of the Farewell Formation, from 63 to 56 Ma, vanished due to deposition between the Oligocene and the recent era and was encountered at a depth of 3054–3334 m in the Kupe-4 well.

4.2 Reservoir characterization

4.2.1 Seismic interpretation

Seismic interpretation makes use of seismic volume to describe the structural features and the seismic facies observed. The seismic section shown in Fig. 10 was

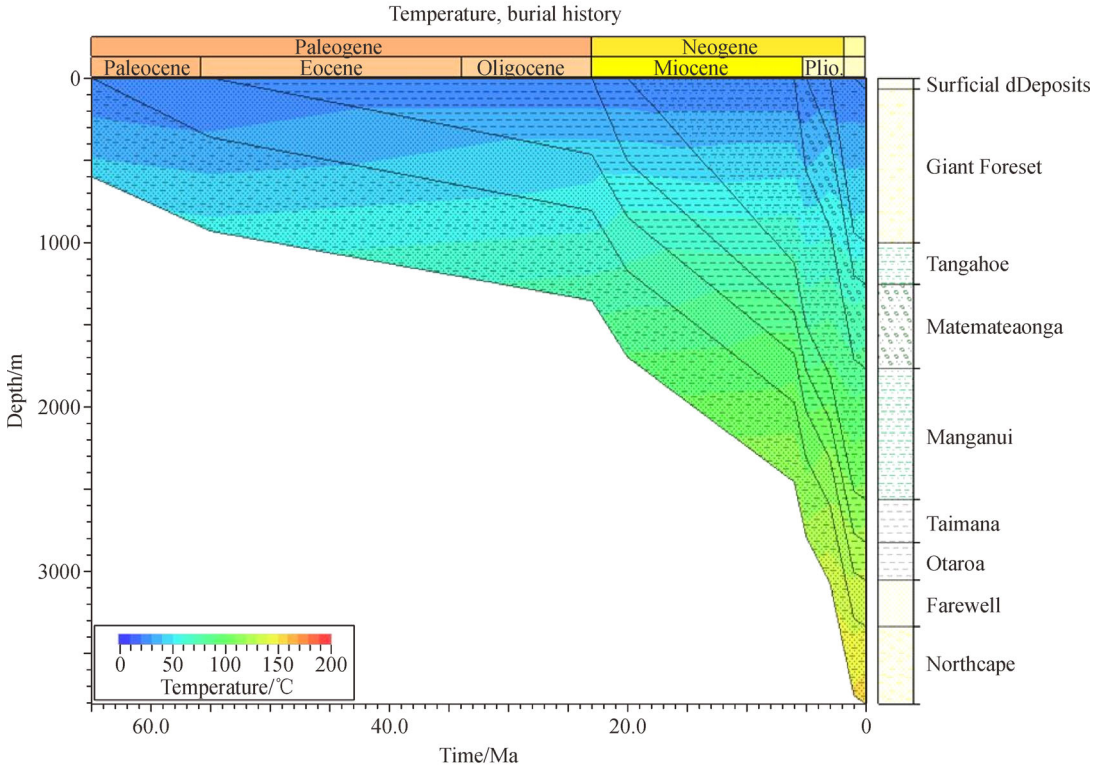

Fig. 9 Burial history diagram of Kupe-4 well representing the burial depth of the reservoir formation and corresponding temperatures.
Burial history diagram of Kupe-4 well representing the burial depth of the reservoir formation and corresponding temperatures.

interpreted by marking 5 depositional packages (indicated by variable colors P1-P5) and two horizons (*H*1 and *H*2), indicating the Farewell Formation (black color) and the Otaraoa Formation (blue color). The well log correlation of the reservoir package within different wells is shown in Fig. 11. The terminus of the first depositional sequence is marked at 800 ms (by purple color) and shows high-angle normal faults along with horst and grabens. This depositional package encloses multiple horizons within it. The second sequence was observed between 800 and 1100 ms (marked by pink color). This sequence shows the structural features of an extensional regime. The continuity of the fault trends is apparent in the second sequence. This continuity in the structural trend is indicated by dashed fault lines. The base of the third depositional sequence is marked by the green color at approximately 1500 ms. This depositional package exhibits more compartmentalization by high-angle normal faults. The base of the fourth depositional episode extends from 2200 to 2500 ms. Due to poor resolution, it was not easy to select faults within this package. The observed faults reflect high-angle normal faults. This depositional sequence terminates above the Otaraoa Formation (top seal). The last depositional package extends between 2500 and 3400 ms, as shown by the red color boundary in Fig. 10. Two horizons were also selected within this depositional package: the Otaraoa and Farewell Formations (blue and black markers, respectively). This sequence can easily be segregated into contractional and extensional zones. The strata are squeezed and exhibit thickening, indicating contractional domination, whereas the thinning of the strata indicates the domination of an extensional regime. The squeezed zone indicates the presence of reverse faults, whereas the extensional zone indicates high-angle normal faults, horst and graben features, and flower structures.

The structural interpretation indicated the complex nature of faulting within the reservoir package. These faults not only cause deformation within the sedimentary basin but also influence hydrocarbon trapping and migration, thereby developing the potential reservoir characteristics. Based on seismic reflection frequency and amplitude continuity (Weimer et al., 1988), three seismic facies can be easily determined within the seismic volume. These three facies are continuous and high-amplitude reflections, variable-discontinuous amplitude reflection, and chaotic configuration.

4.2.2 Well log analysis

The well-log-based petrophysical evaluation incorporated data from four wells, namely, Kupe-1, Kupe South-3B, Kupe-7ST, and Kupe South-8, using Interactive Petrophysics software. The well-log analysis was divided into qualitative and quantitative interpretations. The qualitative

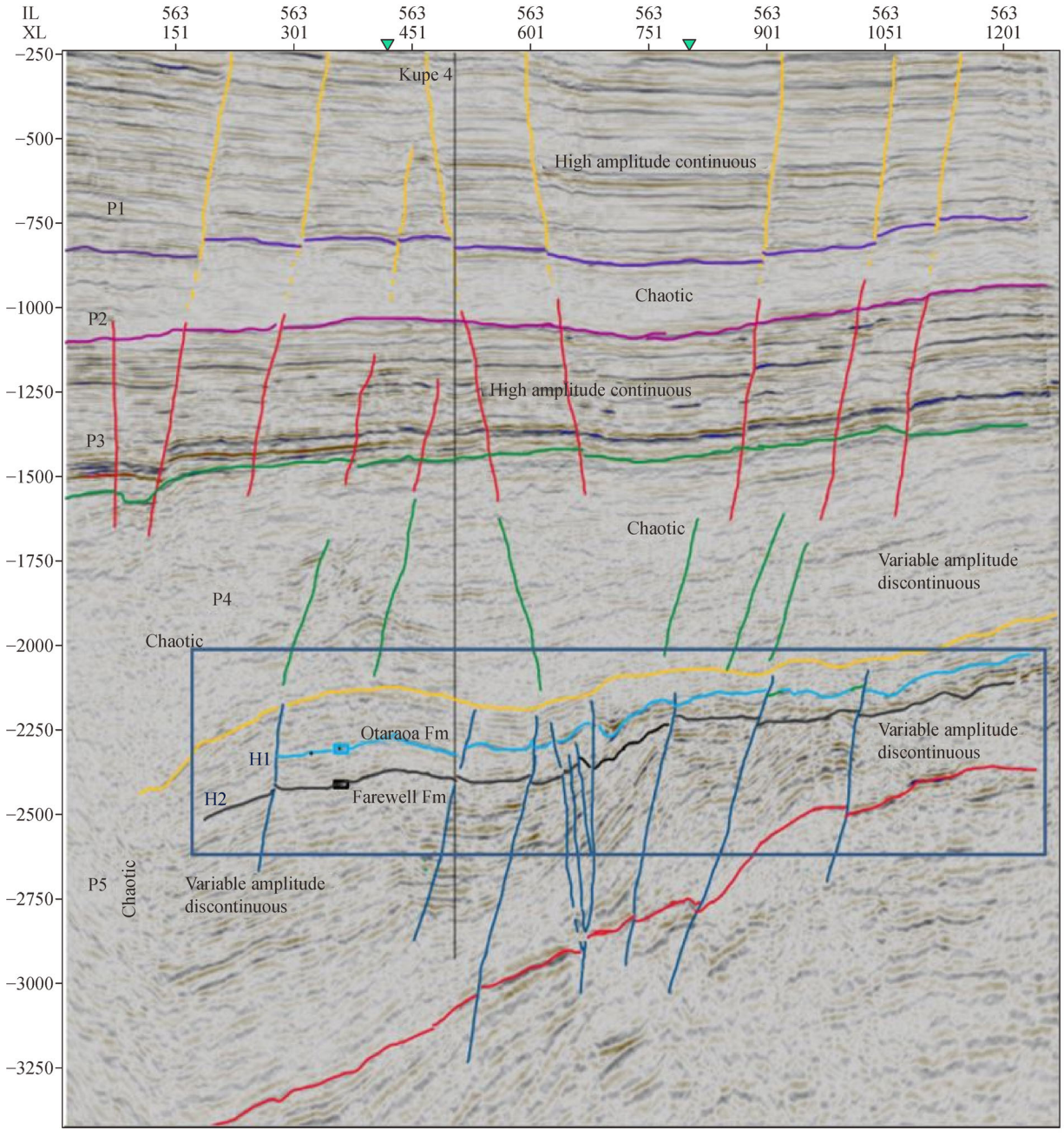

Fig. 10 The seismic section derived from 3D seismic volume of Kupe Field indicating multiple depositional sequences (P1-P5), multiple structural features and the identified seismic facies. The blue rectangle shows the reservoir package (later used for modeling) showing the seal (Otaraoa Formation-H1) and the reservoir (Farewell Formation-H2).

interpretation indicated the lithological content, type of porosity, and type of shale habitat, whereas quantitative estimation indicated the percentage of important petrophysical parameters, including the volume of shale, porosity and its types, water wetness, and the hydrocarbon-bearing within the reservoir formation. To identify the lithology of the reservoir, gamma-ray log values were plotted against neutron porosity values. Figures 12(a) and 12(b) show the reservoir formation in Kupe 1 and Kupe South 3B, comprising shaly sand, with some data clusters within the clean sand range. Traces of carbonate can also be seen within the cross plot. The type of shale habitat inside the pore space is reflected using the neutron log versus the density log cross-plot. Figure 12(c) indicates a dispersed shale habitat within the Kupe South 8 well, which can impact the calculations of effective porosity and fluid saturation. Therefore, to overcome the impact of dispersed shale in the water and hydrocarbon calculations,

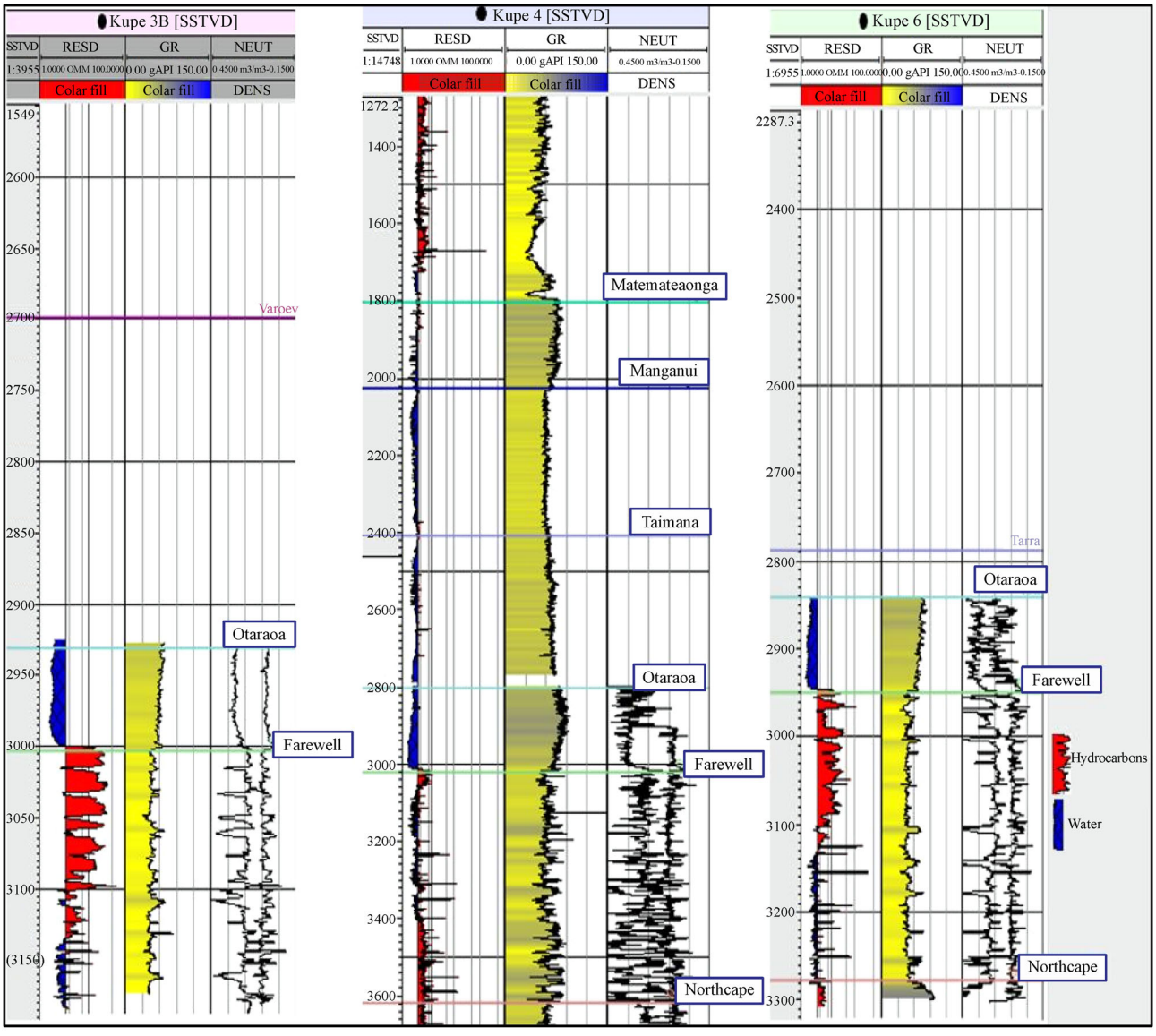

Fig. 11 Well correlation established between Kupe 3B, Kupe 4 and Kupe 6 encountering the Farewell Formation at variable depths.

the dual water saturation model was used. The distinction between the intergranular and secondary porosities was determined by plotting sonic log versus a combination of neutron and density log. Figure 12(d) shows the presence of both intergranular and secondary type porosities within the Kupe 7-ST well. Quantitative interpretations, from the wells examined in the present study for petrophysical evaluation, applied a 50% shale cut off, 50% water saturation cut off, and 10% porosity cut off. This means that the analyses considered the reservoir intervals with less than 50% shale volume, greater than 10% porosity, and more than 50% of hydrocarbon saturation. Table 3 indicates the drilled intervals striking the Farewell Formation at variable depths. The findings reveal that net sand thickness ranged from 126 to 192.5 m, whereas the net pay thickness ranged between 64.9 and 85 m. Similarly, total, and effective porosities ranged from 17.5% to 24.4% and 15.1% and 21.7%, respectively. The volume of shale was estimated to be between 14.7% and 19.3%, whereas hydrocarbon saturation was estimated to range between 62.7% and 70.1% (Table 3).

4.2.3 3D structural and petrophysical modeling

The volume-based modeling algorithm was used to establish the 3D structural model by incorporating the seismic volume stacked in time, well deviation, check shot surveys, and well log data using Petrel 2013.7 software. After the horizon marking and fault interpretation, three surfaces and their corresponding faults were used as a focus to develop the 3D structural model. To establish a correct model, the selected seismic time section between

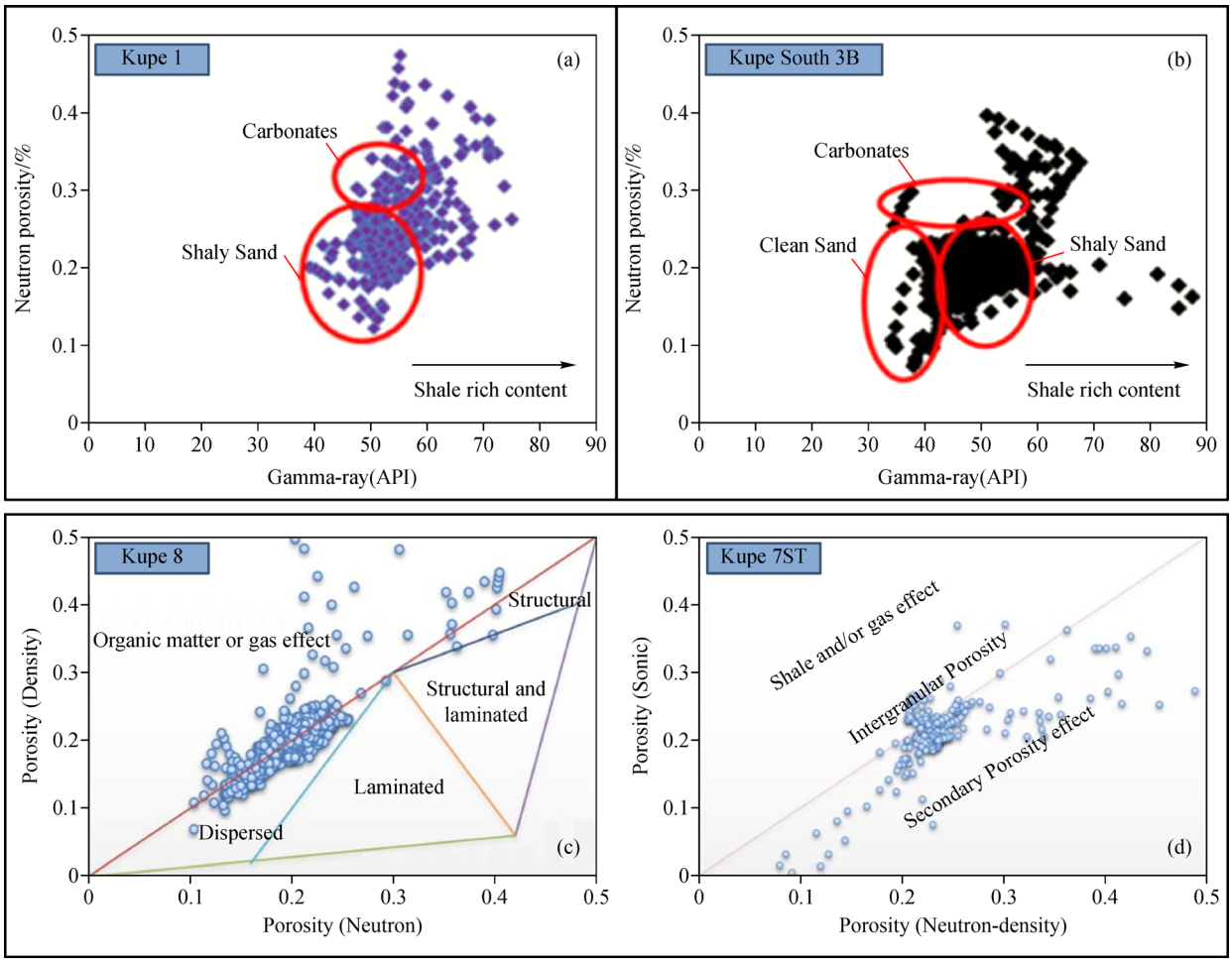

Fig. 12 The Gamma-ray log versus Neutron porosity plot (a) for Kupe-1 well and (b) Kupe 3B well, clearly indicates that the Farewell Formation has relatively higher gamma ray values revealing the shaly sand as dominant lithological content within the Farewell Formation with the presence of carbonates and shale rich contents. The cross plot (c) Neutron porosity versus density porosity indicates dispersed shale habitat for Kupe 8 well and (d) the Neutron-density porosity versus sonic porosity indicates the presence of intergranular and secondary porosities within the Kupe 7-ST.

2000 and 2450 ms was converted into a depth section using a velocity model. The generation of the velocity model converts the selected zones to a depth of 2500–3200 m, as shown in Fig. 13. The model used two zones and three horizons, namely, the Otaraoa Formation (seal), the Farewell Formation (reservoir), and the top of the North Cape Formation (Fig. 13). The model also shows the scars of the 45 faults selected within the reservoir package; the southern part is elevated as compared to the northern part in the structural model. The fault density is more apparent in the center and south of the structural model. The 3D structural model was interpreted as a combination of extensional and inversion structures, with thickening of strata toward the south and thinning toward the north. The distribution of faults throughout the reservoir package indicated the presence of trapping mechanisms, indicative of reservoir characteristics.

Sequential Gaussian simulation was applied to develop two 3D petrophysical models, namely the Gamma-ray model and the hydrocarbon saturation model. The reason for designing only these four models was to obtain a clear indication of the spatial distribution of major lithological content as well as hydrocarbon saturation. The gamma-ray model indicated the presence of clay minerals within the formation (Erlström and Sopher, 2019), and designing a 3D model will help differentiate between shale and sand zones. The incorporation of well log data includes gamma-ray and resistivity values within the 3D seismic volume for the well, along with their locations. The spatial distribution of gamma-ray and resistivity values is established once we reach the griding stage during the development of petrophysical models. The distribution of the sampled wells within the seismic volume influences the petrophysical modeling. Figure 14 shows that the gamma-ray values ranged between 40 and 120 API. The 3D gamma-ray model demonstrated that most of the 3D volume

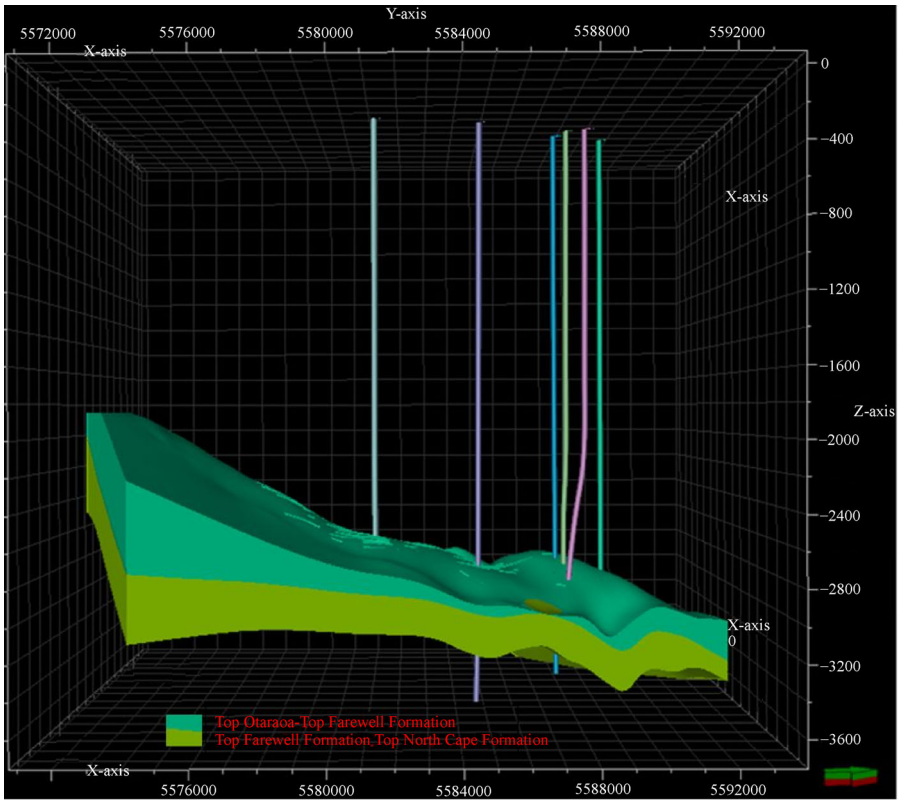

Fig. 13 The 3D structural model for the reservoir package including tops of Otaraoa, Farewell and North Cape Formations along with the fault traces and drilled wells within the Kupe Field.

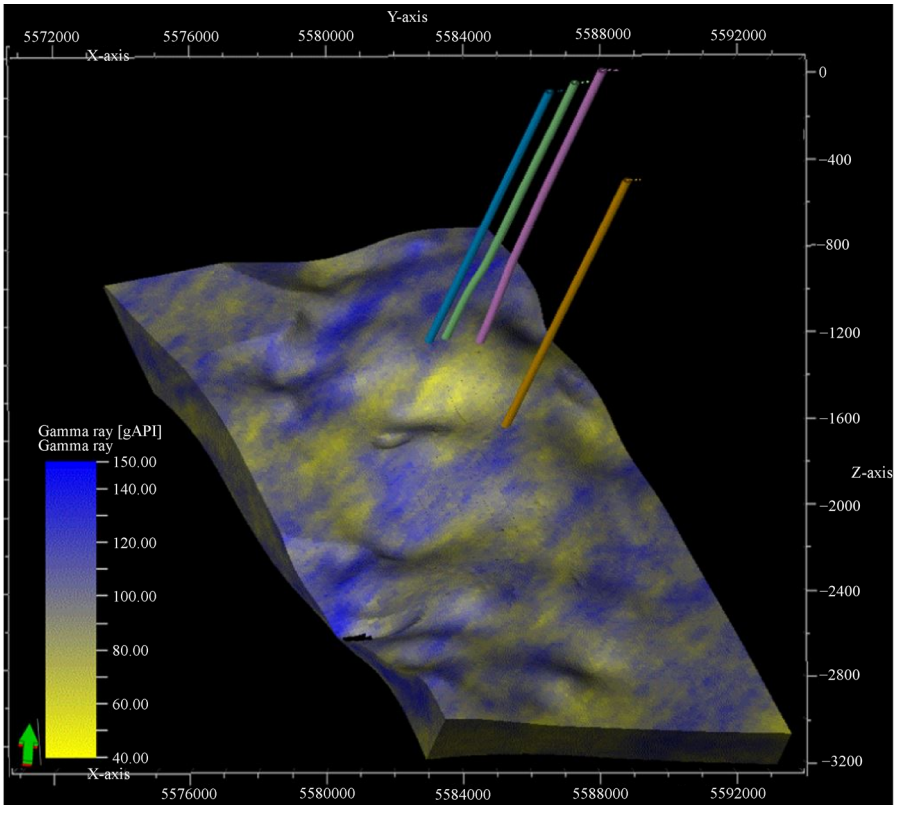

Fig. 14 3D Gamma ray model of the reservoir formation showing zones of high and low values thus differentiating between the shale and sand regions, respectively. The model clearly shows the shaly sand nature of Farewell Formation.

exhibited higher gamma-ray values and, thus, indicates the presence of shale (blue color). Some spots exhibited relatively lower values (indicated by the yellow color) and were identified as sand zones. Most of the drilled wells indicated sand rich to shaly sand zones. This agrees with the log of gamma-ray versus neutron-porosity cross plot, which shows that the lithological content ranged from clean sand to shaly sand. The deep resistivity logs help in differentiating the hydrocarbon-bearing and non-hydrocarbon bearing zones (Chongwain et al., 2019). The 3D resistivity model (Fig. 15) is an indirect approach to present the zones with higher and lower resistivity within the seismic volume. The 3D resistivity model indicated very high resistivity within the seismic volume. The resistivity model, combined with the gamma-ray and effective porosity models (Fig. 16), can present a better picture of the prospective zones within the study area. The 3D effective porosity model demonstrated that the variable distribution of porosity values ranged between 10% and 30%. Regions within the distribution of well logs indicate effective porosity between 15% and 25%, revealing a very good reservoir character. The gamma-ray, resistivity, and porosity models agreed with each other, indicating zones with a higher prospect. The 3D hydrocarbon saturation model (Fig. 17) indicated hydrocarbon saturation ranging up to 70%. Zones with yellowish-green color indicate higher hydrocarbon saturation. The wells examined in this study and represented in the 3D model were drilled within the regions of higher hydrocarbon saturation. Furthermore, there are certain zones of higher hydrocarbon. saturation and these can be used for drilling in the future. The gamma-ray and hydrocarbon saturation models were inversely correlated; higher shaly areas exhibited lower hydrocarbon saturation and vice versa. The range of hydrocarbon saturation in the 3D model is in good agreement with the values summarized in Table 3. The presence of multiple hydrocarbon zones within the hydrocarbon saturation simulation implies that the Farewell Formation is a good reservoir. The petrophysical models present the reservoir characteristics of the Farewell Formation.

5 Summary and conclusions

This comprehensive study, which integrated different techniques for the characterization of source and reservoir rocks, demonstrated the following:

1) Geochemical data analysis of samples derived from the Farewell Formation exhibited fair-to-very good hydrocarbon generation potential, and the quality and maturity of the organic matter were fair-to-excellent and immature-to-mature, respectively. Type II-III (oil-gas prone) and type III kerogens (gas prone) were apparent, indicating a good source rock character.

2) Structural interpretations indicated complex structural settings as both compressional and extensional regimes were apparent from the seismic volume. The younger strata

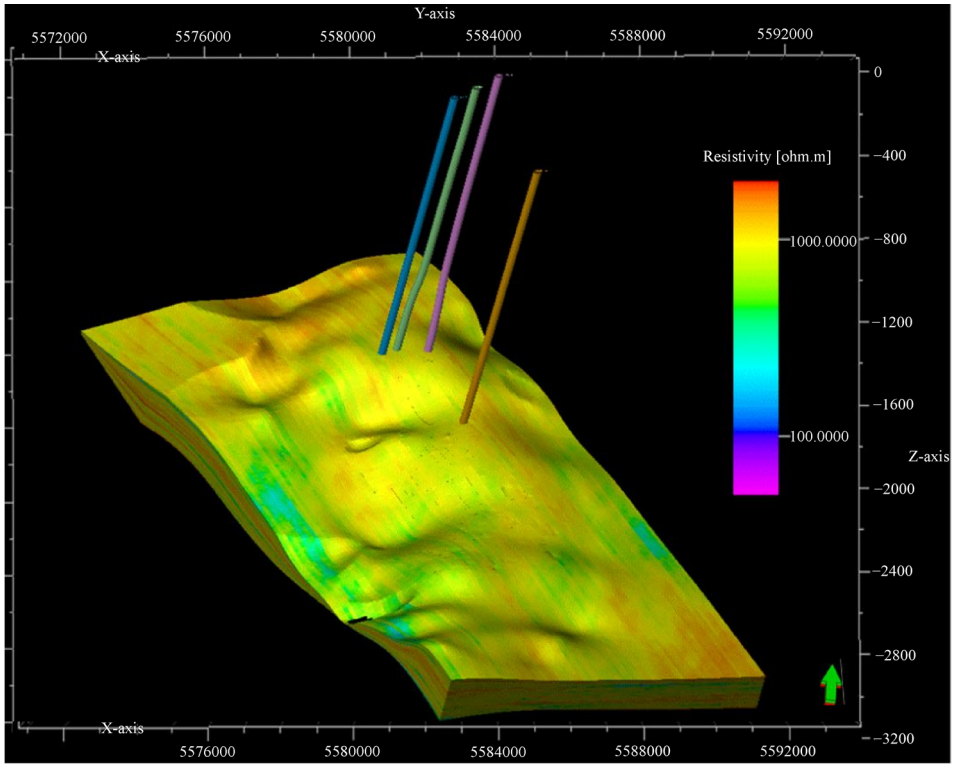

Fig. 15 The resistivity model for the Farewell Formation in the Kupe Field showing high resistivity values near the drilled wells.

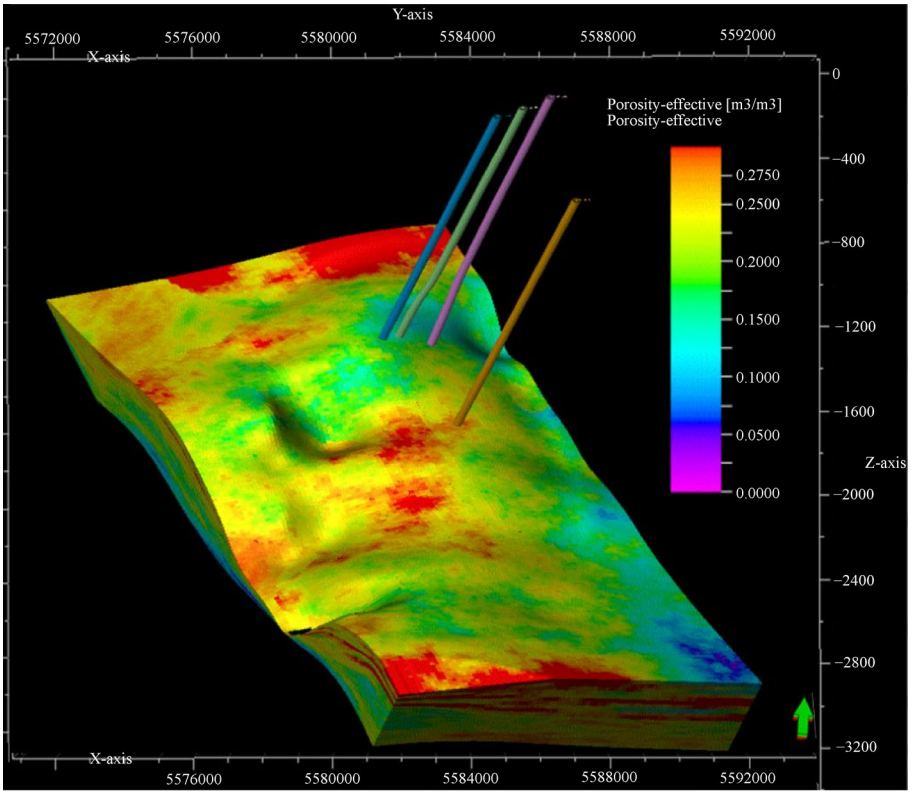

Fig. 16 3D effective porosity model revealing spatial distribution of effective porosity with high and low values along with the drilled wells.

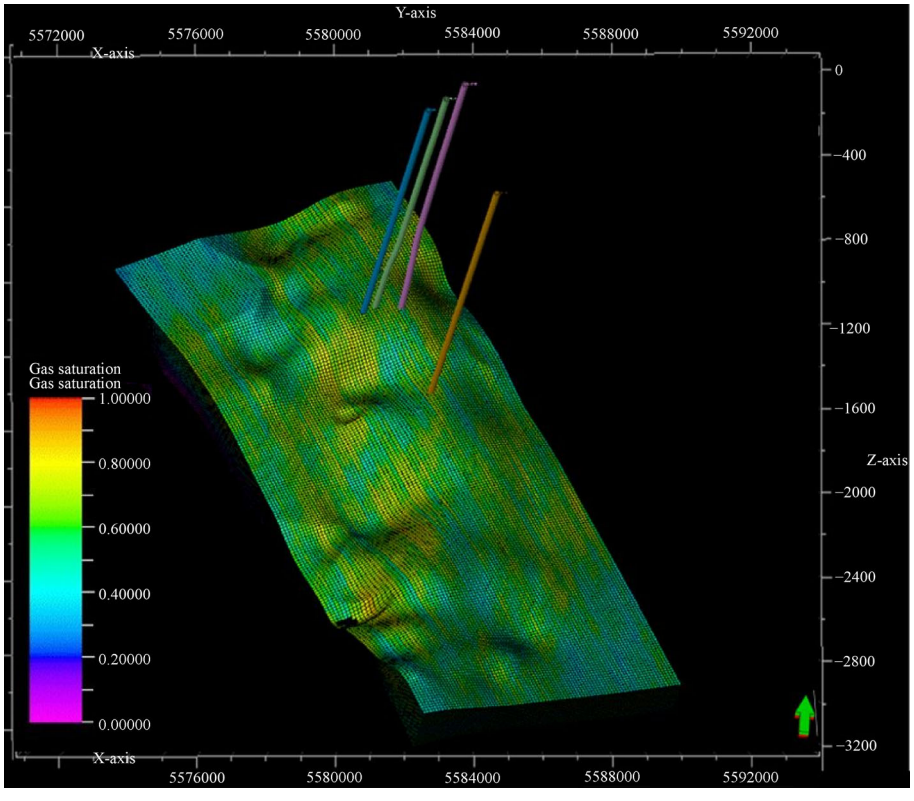

Fig. 17 3D hydrocarbon saturation model of the reservoir formation showing significant distribution of hydrocarbons.

Table 3 Quantitative description of multiple petrophysical parameters evaluated by well log analyses

Well Name	Gross Thickness/m			Net Sand		Net Pay		Porosity ϕ/%		V_{sh}/%	S_w/%	S_H/%
	Top	Base	Thickness	Thickness/m	N:G/%	Thickness/m	N:G/%	ϕ_T	ϕ_e			
Kupe-1	3190	3650	460	140	30.4	85.0	18.5	23.7	20.8	18.9	36.6	63.4
Kupe S-3B	3230	3445	215	126	58.6	72.3	33.6	24.4	21.7	19.3	37.3	62.7
Kupe 7-ST	3187	3495	308	132	42.3	76.1	24.8	17.5	15.1	14.7	29.9	70.1
Kupe S-8	3513	3800	287	192.5	67.1	64.9	22.6	20.4	19.2	17.7	38.4	61.6

Notes: V_{sh} is the volume of the shale, ϕ_T is the total porosity, ϕ_e is the effective porosity, S_w is the water saturation, and S_H is the hydrocarbon saturation estimated after applying 50% *V*sh cut off, 50% water saturation, and 10% porosity cut off.

predominantly indicated normal faulting, whereas the reservoir package (seal and reservoir formation) demonstrated the presence of both normal and reverse faulting. The presence of high-angle faults indicated the trapping mechanisms within the reservoir package, provided the faults are duly sealed. It can be reasonably inferred that the faults are sealed because the field is already in production, implying that a good trapping mechanism exists, which is an important reservoir feature.

3) The well-log-based evaluation indicated thick sand zones, pay zones, and significant net-to-gross ratios. This analysis demonstrated that shaly sand is the dominant lithological content, along with intergranular and secondary pore spaces. The pore spaces within the sand zones have moderate-to-low shale volume (14.7%–19.3%), moderate water saturation (29.9%–38.4%), and substantial hydrocarbon saturation (61.6%–70.1%). The petrophysical parameters revealed using the well log-based evaluation reflect valuable reservoir properties.

4) The 3D structural model indicated the seal and reservoir horizons and the distribution of structural features within the reservoir package. The 3D gamma-ray log model indicated the presence of shaly and sandy zones and verified the findings related to the lithological character of the reservoir formation.

5) The 3D resistivity and porosity models complemented the gamma-ray model and improved our understanding of reservoir potential.

6) The 3D petrophysical model demonstrated zones with significant distributions of hydrocarbon saturation within the Kupe Field.

7) The application of 1D and 3D modeling schemes, along with other geological and geophysical methods, improved our understanding that the Farewell Formation works as a self-sourced reservoir within the Kupe Field.

References

Adelu A O, Aderemi A A, Akanji A O, Sanuade O A, Kaka S L I, Afolabi O, Olugbemiga S, Oke R (2019). Application of 3D static modeling for optimal reservoir characterization. J Afr Earth Sci, 152: 184–196

Anyiam O A, Eradiri J N, Mode A W, Okeugo C G, Okwara I C, Ibemesi P O (2020). Sequence stratigraphic analysis and reservoir quality assessment of an onshore field, Central Swamp Depobelt, Niger Belt Basin, Nigeria. Arab J Geosci, 12(24): 791

Ali M, Abdelhady A, Abdelmaksoud A, Darwish M, Essa M A (2019). 3D static modelling and petrographic aspects of the Albian/Cenomanian Reservoir, Komombo Basin, Upper Egypt. Nat Resour Res, 29(2): 1259–1281

Armstrong P A, Chapman D S, Funnell R H, Allis R G, Kamp P J J (1996). Thermal modelling and hydrocarbon generation in an active margin basin: Taranaki Basin, New Zealand. AAPG Bull, 80: 1216–1241

Barker C (1974). Pyrolysis techniques for source rock evaluation. AAPG Bull, 58: 2349–2361

Burrus J, Kuhfuss A, Doligez B, Ungerer P (1991). Are numerical models useful in reconstructing the migration of hydrocarbons? A discussion based on the Northern Viking Graben. Geol Soc Lond Spec Publ, 59(1): 89–109

Chongwain G M, Osinowo O O, Ntamak-Nida M J, Biouele S E A, Nkoa E N (2019). Petrophysical characterization of reservoir intervals in well-X and well-Y, M-Field, offshore Douala Sub-Basin, Cameroon. J Pet Explor Prod Technol, 9(2): 911–925

Erlström M, Sopher D (2019). Geophysical well log motifs, lithology, stratigraphical aspects and correlation of the Ordovician succession in the Swedish part of the Baltic Basin. Int J Earth Sci, 108(4): 1387–1407

Espitalie J, Laporte L J, Madec M, Marquis F, Leplat P, Paulet J, Boutefeu A (1977). Rapid method of characterization of sea rocks, their oil potential and their degree of evolution. Rev Inst Fran. Pétrole, 32: 32–42 (in French)

Franzel M, Back S (2019). Three-dimensional seismic sedimentology and stratigraphic architecture of prograding clinforms, central Taranaki Basin, New Zealand. Int J Earth Sci, 108(2): 475–496

Hakimi M H, Shalaby M R, Abdullah W H (2012). Diagenetic characteristic and reservoir quality of the Lower Cretaceous Biyadh sandstones at Kharir oilfield in the western central Masila Basin, Yemen. J Asian Earth Sci, 51: 109–120

Haque A K M E, Islam M A, Ragab Shalaby M O H A M E D R (2016). Structural modelling of the Maui Gas Field, Taranaki Basin, New Zealand. Pet Explor Dev, 43(6): 965–975

Hemming-Sykes S (2011). The influence of faulting on hydrocarbon migration in Kupe area, south Taranaki Basin, New Zealand. Dissertation for Master's Degree. Wellington: Victoria University of Wellington

Higgs K E, Crouch E M, Raine J I (2017). An interdisciplinary approach

to reservoir characterization: an example from the early to middle Eocene Kaimiro Formation, Taranaki Basin, New Zealand. Mar Pet Geol, 86: 111–139

Higgs K E, King P R, Raine J I, Sykes R, Browne G H, Crouch E M, Baur J R (2012). Sequence stratigraphy and controls on reservoir sandstone distribution in an Eocene marginal marine-coastal plain fairway, Taranaki Basin, New Zealand. Mar Pet Geol, 32(1): 110–137

Ilg B R, Hemmings-Sykes S, Nicol A, Baur J, Fohrmann M, Funnell R, Milner M (2012). Normal faults and gas migration in an active plate boundary, southern Taranaki Basin, offshore New Zealand. AAPG Bull, 96(9): 1733–1756

Islam M A, Yunsi M, Qadri S M T, Shalaby M R, Haque A K M E (2020). Three-dimensional structural and petrophysical modeling for reservoir characterization of the Mangahewa Formation, Pohokura Gas-Condensate Field, Taranaki Basin, New Zealand. Nat Resour Res,

Johnston J H, Collier R H, Collen J D (1990). What is the source of Taranaki oils? Geochemical biomarkers suggest it is very deep coals and shales. In: Proceedings of New Zealand Oil Exploration Conference 1989, Wellington

Jumat N, Shalaby M R, Aminul Islam M (2018). Integrated reservoir characterization of the Paleocene Farewell Formation, Taranaki Basin, New Zealand, using petrophysical and petrographical analyses. J Pet Explor Prod Technol, 8(3): 685–701

Killops S D, Woolhouse A D, Weston R J, Cook R A (1994). A geochemical appraisal of oil generation in the Taranaki Basin, New Zealand. AAPG Bull, 78: 1560–1585

King P R, Thrasher G P (1996). Cretaceous−Cenozoic geology and petroleum systems of the Taranaki Basin, New Zealand. In: Institute of Geological and Nuclear Sciences Monograph, vol.13 (2). Institute of Geological & Nuclear Sciences, Lower Hutt

Knox G J (1982). Taranaki Basin, structural style and tectonic setting. N Z J Geol Geophys, 25(2): 125–140

Martin K R, Baker J C, Hamilton P J, Thrasher G P (1994). Diagenesis and reservoir quality of Paleocene sandstones in the Kupe South Field, Taranaki Basin, New Zealand. AAPG Bull, 78(4): 624–643

Mukhopadhay P K (1994). Petrographic and molecular characterization and its applications to basin Modelling. In: Mukhopadhyay PK, Dow WG, eds. Vitrinite reflectance as a maturity parameter: applications and limitations. American Chemical Society, Washington DC

Osinowo O O, Ayorinde J O, Nwankwo C P, Ekeng O M, Taiwo O B (2018). Reservoir description and characterization of Eni field offshore Niger Delta, southern Nigeria. J Pet Explor Prod Technol, 8(2): 381–397

Osli L N, Shalaby M R, Islam M A (2018). Characterization of source rocks and depositional environment, and hydrocarbon generation modelling of the Cretaceous Hoiho Formation, Great South Basin, New Zealand. Petrol Coal, 60(2): 255–275

Peters K E (1986). Guidelines for the evaluating petroleum source rock using programmed pyrolysis. AAPG Bull, 70(3): 318–329

Peter K E, Cassa M R (1994). Applied source rock geochemistry. In: Magoon L, Dow WG, eds. The petroleum system-from source-trap: AAPG Memoir, 60: 93–120

Qadri S M T, Shalaby M R, Islam M A, Hoon L L (2016). Source rock characterization and hydrocarbon generation modeling of the Middle to Late Eocene Mangahewa Formation in Taranaki Basin, New Zealand. Arab J Geosci, 9(10): 559

Qadri S M T, Islam M A, Shalaby M R, Eahsan ul Haque A K M (2017). Seismic interpretation and structural modelling of Kupe Field, Taranaki Basin, New Zealand. Arab J Geosci, 10(14): 295

Qadri S M T, Islam M A, Shalaby M R (2019a). Three-dimensional petrophysical modelling and volumetric analysis to model the reservoir potential of the Kupe Field, Taranaki Basin, New Zealand. Nat Resour Res, 28(2): 369–392

Qadri S M T, Islam M A, Shalaby M R (2019b). Application of well log analysis to estimate the petrophysical parameters and evaluate the reservoir quality of the Lower Goru Formation, Lower Indus Basin, Pakistan. Geo-mech. Geophys. Geo-energ. Geo-resour, 5: 271–288

Qadri S M T, Islam M A, Shalaby M R, Abdel Aal AK (2020). Reservoir quality evaluation of the Farewell sandstone by integrating sedimentological and well log analysis in the Kupe South Field, Taranaki Basin, New Zealand. J Petrol Explor Prod Technol

Sarma M, Kellet R, Pryde S, Reynolds G (2014). Petroleum Systems Modelling: Evaluation of the Eltham Area (PEP 51150), Onshore Taranaki Basin. Wellington: New Zealand Corp

Seyyedattar M, Zendehboudi S, Butt S (2020). Technical and non-technical challenges of development of offshore petroleum reservoirs: Characterization and production. Nat Resour Res, 29(3): 2147–2189

Shalaby M R, Hakimi M H, Abdullah W H (2011). Geochemical characteristics and hydrocarbon generation modelling of the Jurassic source rocks in Shoushan Basin, north Western Desert, Egypt. Mar Pet Geol, 28(9): 1611–1624

Sykes R, Volk H, George S C, Ahmed M, Higgs K E, Johansen P E, Snowdon L R (2014). Marine influence helps preserves the oil potential of the coaly source rocks: Eocene Mangahewa Formation, Taranaki Basin, New Zealand. Org Geochem, 66: 140–163

Sykes R, Snowdon L R (2002). Guidelines for assessing the petroleum potential of the coaly source rocks using rock-eval pyrolysis. Org Geochem, 33(12): 1441–1455

Thompson J G (1982). Hydrocarbon source rock analyses of Pakawau Group and Kapuni Formation sediments, northwest Nelson and offshore South Taranaki, New Zealand. N Z J Geol Geophys, 25(2): 141–148

Tissot B P, Welte D H (1984). Petroleum Formation and Occurrence. 2nd ed. Berlin: Springer

Wapples D W (1980). Time and temperature in petroleum formation: application of Lopatin's method to petroleum exploration. AAPG Bull, 2(6): 916–926

Wapples D W (1994). Maturity modelling: thermal indicators, hydrocarbon generation, and oil cracking. AAPG Mem, 60: 285–306

Weimer R J, Rebne C A, Davis T L (1988). Geologic and seismic models, muddy sandstone, Lower Cretaceous, Bell Creek-Rocky Point area, Powder River basin, Montana and Wyoming. In: Diedrich R, Dyka M, Miller W. eds. Eastern Powder River basin-Black Hills: Wyoming Geological Association 39th Field Conference Guidebook, 147–160

Wyllie M R J (1963). The Fundamentals of Well Log Interpretations. New York: Academic Press